UNIVERSITY OF TWENTE

MASTER APPLIED PHYSIS / MECHANICAL ENGINEERING

Validating the effect of vertically staggered wind turbines in the entrance region of extended windfarms

Author:
M.G. Arendshorst
s1498630

External supervisor:
Dr. K. Chauhan

Internal supervisors:
Dr. D. Krug
Dr. Ir. A. Van Garrel

Duration and credit points:
20 weeks
30 EC

July 23, 2019

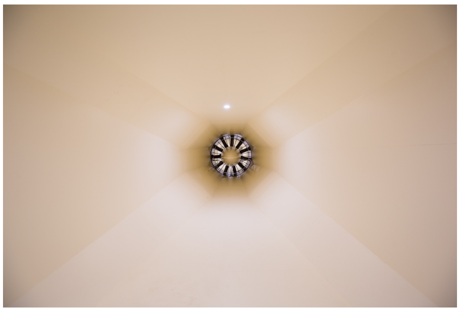

THE UNIVERSITY OF SYDNEY

UNIVERSITY OF TWENTE.

Summary

This internship is part of my double masters degree Applied Physics/Mechanical Engineering at the University of Twente. I went to the School of Civil Engineering within the University of Sydney to design a scaled-down wind turbine post that I thereafter used to study the effect of vertically staggered wind turbines within the entrance region of a large wind farm in the Boundary Layer Wind Tunnel. The turbine posts consists of four features: an array of flat faces that allow vertical staggering without the need of multiple different sized wind turbines, a flat surface in combination with an inclined hole on which a strain gauge can be applied and the strain gauge leads can be fed through, a slot that enables the turbine posts to bend more near the base of the post and a threaded section with two flats on either side that are used for positioning and aligning the turbine post in the wind tunnel. The research was done to validate the results from Large Eddy Simulation (LES) on vertically staggered wind farms. The study suggested that elevating the odd numbered turbine rows increases the power production of the entrance region of a large wind farm more than the entrance region in a wind farm in which the odd numbered turbine rows were lowered under certain conditions. I found that the wind farm in which the odd numbered turbine rows were lowered performed better instead, although under slightly different conditions, such as a higher incoming freestream velocity and a smaller turbine spacing. Another part of my internship was tutoring a third year Fluid Mechanics course to students that are doing their third year of studying Civil Engineering at the University of Sydney.

Contents

1 A smarter wind turbine post design

1.1 Problem Definition

1.1.1 Problem scope

Strain gauges are commonly used to measure the deformation of a material due to a load on an object. Effective and accurate strain gauge measurements are key to delivering good test results. However, strain gauge signals are noisy and signals with a low signal-to-noise ratio give more accurate results. Therefore large deformations give more accurate results than small deformations. Moreover, strain gauges applied to wind turbine posts are exposed to the wind flow in the wind tunnel which causes the leads to break easily. Also, testing wind farm setups with vertical staggering is cost and labour intensive due to the large number of different sized posts within the setup and the time required to prepare and install a particular setup.

1.1.2 Technical review

The forces and loads exerted on an object cannot be measured directly. Some kind of device needs to be used in order to measure the forces and loads. Strain gauges are typically used for this purpose in experiments concerning scaled-down wind turbines. A strain gauge consists of a metallic foil pattern which is strain sensitive. Due to tension (or elongation of the object) the area of the foil pattern increases so that the cross-sectional area of the wire in the foil pattern decreases causing an increase in resistance in the wire. Due to compression (or shortening of the object), the exact opposite happens: the area of the foil pattern decreases which results in a thicker foil pattern wire causing a decrease in resistance in the wire. Any load results in a deformation of the object and can thus be converted into an electric signal using a strain gauge.

Every post has two strain gauges: one on the side of the post that is facing upstream and one that is facing downstream. Together they make a leg of an electrical bridge circuit. This leg is combined with another leg consisting of two known resistors with equal resistance to the strain gauges to form a complete bridge circuit, also known as a Wheatstone bridge. An illustration of a Wheatstone bridge with two strain gauges can be seen in Figure 2. Any deformation of the wind turbine post will result in a change of resistance of the strain gauges causing an unbalance in the Wheatstone bridge. This unbalance results in a voltage change in the circuit characteristic to the change in resistance and thus to the applied external force that causes the deformation. The double strain gauge configuration eliminates any temperature effects on the strain and the output signal is twice as high as the output of a single strain gauge.

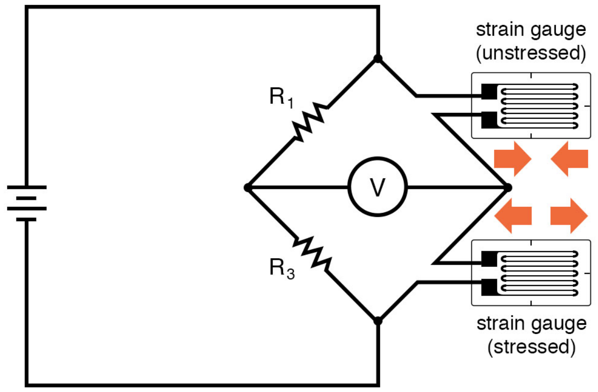

Figure 2: A half bridge strain gauge circuit. Adapted from [1].

Strain is directly related to the Young's modulus. This means that materials with a low Young's modulus will experience more strain than a material with a high Young's modulus under the same applied load.

1.1.3 Design requirements

The main design requirement is that the strain signal of the new design is 20% higher than than the strain signal of a solid post under the same applied force so that the noise contributes less to the signal. Furthermore, the strain gauge leads can only be exposed to the wind flow for less than 5 mm so that the risk of breaking them is minimal. Also, the position of the turbine disk on the turbine post should be adjustable so that four different levels of vertical staggering of $H_\mathrm{d} = D/10$ can be applied while also no staggering in the vertical direction is possible ($H_\mathrm{d} = 0$). In addition, the turbine post cannot extend above the turbine disk once the turbine disk is attached to the turbine post because it cannot be exposed to the flow above the turbine disk. Lastly, the turbine post cannot move more than 1 mm in the vertical direction in order to prevent the turbine post from be lifted. Use of more than one component can be used for this requirement.

The above requirements are summarised in Table 1.

1.2 Design description

1.2.1 Design selection for testing

A number of functions with possible designs can be found in Appendix B that have been considered to come up with a number of conceptual designs. In the next sections, the final design will be discussed and evaluated.

1.2.2 Overview final design

Figure 3 shows the final design. Every dimension in this design is based on the dimensions of a model turbine disk of diameter $D_\mathrm{m} = 100$ mm and consists of two different sized posts: a short turbine post A and a tall turbine post B. The difference in their designs is the total height of the post. All features are relative either to the top of the post or to the bottom of the post and the dimensions of these features are the same. Therefore, the working principle of the posts will only be described for the short turbine post A. The technical drawings for both turbine posts of the final design can be found in Appendix A.

The posts are 12 mm thick perspex rods that consist of four main features. These features are numbered 1 to 4 in Figure 3. The first feature is an array of five flat faces that provide an anchor point for the turbine disk for different levels of vertical staggering. The second feature consists of a flat surface on which the strain gauge can be applied, an inclined hole above the flat surface that will guide the strain gauge leads into the post and a hole at bottom of the post that acts as an exit for the leads. The third feature is a slot that enables the post to bend more near the base of the post. The fourth feature consists of a threaded section with two flats on either side of the post that can be used to constrain the post in the vertical direction and align the post so that it is facing in the direction of the wind flow, respectively. All of the features will be elaborated on in the next section.

Table 1: Summary of the design requirements.

Metric	Importance	Units	Marginal value	Ideal value
Ratio strain gauge signal	5	%	20	30
Length exposed leads	3	mm	5	5
Levels of vertical staggering	5	-	5	5
Extended rod length	3	mm	2	0
Movement vertical direction	4	mm	0.5	0

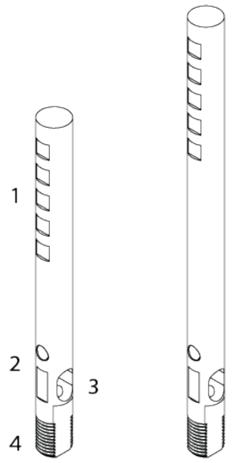

Figure 3: Isometric view of posts A and B. Post A is 131 mm tall and post B 171 mm.

1.2.3 Detailed description

The first feature is an array of five flat faces with dimensions 6×6 mm and depth of 1 mm. The distance from the top of one face to the top of the its neighbouring faces is 10 mm so that vertical staggering of $H_\text{d} = D_\text{m}/10$ can be achieved when a turbine disk of $D_\text{m} = 100$ mm is used in experiments. The top face of the short post and the bottom face of the tall post are on the same horizontal level. The distance between the centre of the bottom face and the top of the post is 50 mm so that only a small portion of the turbine post is exposed to the wind flow at the minimum level of vertical staggering when a disk diameter $D_\text{m} = 100$ mm is used.

The second feature consists of a 12×4.8 mm flat surfaces with a depth of 0.5 mm on the upstream and downstream side of the post on which a strain gauge can be applied. In general, strain gauges are smaller than the flat surface, but a slightly bigger surface makes it easier to apply the strain gauges. The leads of the strain gauges are fed through the hole above their respective flat surface. The holes are at a $45°$ angle downward so that the cables can exit through the hole at the bottom of the post.

The third feature is an extruded slot in the form of a rectangle (5×7 mm) with a semicircle ($R = 3.5$ mm) above and below the rectangle. The slot is positioned between the two flat surfaces on which the strain gauges can be applied and it runs parallel to the flat surfaces. The post will be able to deform more around the area of the slot which will potentially increase the strain gauge signal to ensure a higher signal-to-noise ratio.

The fourth feature consists of two flats with a height of 22 mm and a depth of 2 mm and a fine M12 threaded section with a height of 13.90 mm. The two flats are parallel to each other and can be used to align the turbine post in a particular setup. A nut can be used on the threaded section which in combination with the shoulders above the two flats constrain the turbine post in the vertical direction.

1.2.4 Use

This section describes how the design can be used to measure a strain gauge signal on a wind turbine in a wind tunnel experiment. Start off by applying a strain gauge on the flats on either side of the slot. Next, the strain gauge leads are fed through the holes above the flats, downward into the slot and then further down until it exits the post through the bottom hole of the post. Then the post is installed on the floorboard that have holes shaped like the bottom part of the design. The thickness of the floorboard should not exceed 17 mm in order to allow enough room for a nut to hold onto enough threads on the post. Fasten the nut to the threaded section and ensure it is hand tight. Next, install the turbine disk using a right angle clamp onto the turbine post. The height of the turbine disk relative to the floorboard can be adjusted by applying the right-angle clamp onto the different faces at the top of the post. Place the setup in the wind tunnel with the turbine disk facing the wind flow and attach the strain gauge leads to suitable instruments to acquire the data.

1.3 Evaluation

1.3.1 Overview

The ratio between the strain gauge signal of a slotted post and a solid rod will be tested by means of experiments on a prototype of the slotted post and a prototype of the rod. The length of the strain gauge leads that is exposed to the wind flow can be determined easily and will be measured by means of a ruler. The distance between the faces that can be used to apply different amounts of vertical staggering will be measured with a ruler as well. Comparing the technical drawings for post A and post B should show that one of the faces on post A is at the same height as one of the faces of post B. The difference between the top of the post and the turbine disk at the lowest face of the turbine can be determined using simple geometrical relations of the technical drawings. The extend of the possible vertical movement of the post will be tested by inserting the post in a piece of formply with a hole similar to the contour of the bottom of the post and fastening the post onto the formply using a fine threaded M12 nut.

1.3.2 Prototype

The purpose of the prototypes is to test the strain gauge response of a post with a slot and a post without a slot, to measure the length of the exposed strain gauge leads and to determine the amount of movement in the vertical direction. The prototypes are 170 mm rods made of perspex, see Figure 4. The first prototype, from this point on referred to as the normal post, has features 2 and 4 described in section 1.2.3 while the second prototype, the slotted post, has features 2, 3 and 4 described in the same section. Both prototypes have flat faces at the top of the post on which loads can be applied for testing the strain gauge response. The presence of feature 2 makes it possible to measure the length of the exposed leads and feature 4 enables measuring the amount movement in the vertical direction.

Figure 4: (a) Front view of the prototypes illustrating features 2 and 4 described in section 1.2.3 are present on both posts. (b) Side view of the prototypes illustrating feature 3 is present on the left post (slotted post) in the figure and absent on the right post (normal post) in the figure.

1.3.3 Testing and results

The ratio between the strain gauge signals of the slotted post and the normal post can be determined by applying a known load on the posts. This is done by mounting the post in a six-axis load cell (JR3 30AE12A4 100N) that measures the forces and moments in three different directions. After positioning the load cell horizontally, weights can be applied to test the response of the strain gauge signals while also measuring the forces and moments from the load cell. The measured force F_y from the load cell can be plotted against the strain ε, see Figure 5. The figure also shows a fit through the F_y data which is of the form $y = ax$. The resulting force versus strain diagram can be verified by determining the arm a of the forces that are applied and determining M_x/a, in which M_x is the x-component of the moment. This relation is also plotted in Figure 5 for the slotted and the normal post. F_y and M_x/a show similar results. The ratio between the slopes of the fitted data $a_{slot}/a_{normal} \approx 1.27$, i.e. adding a slot to the post increases the strain gauge signal output by 27%.

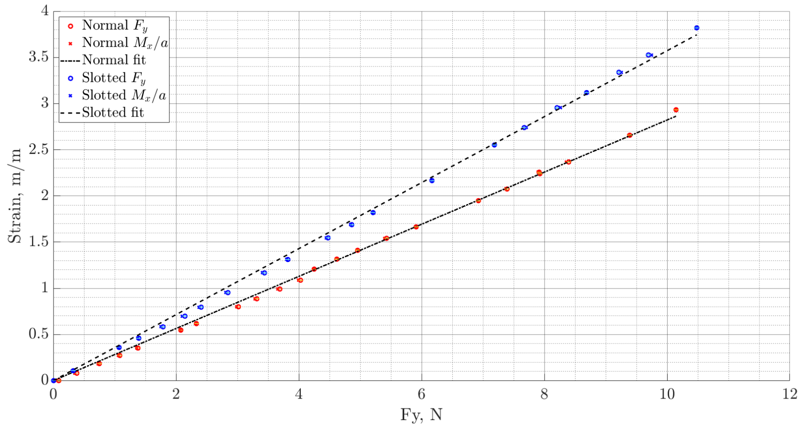

Figure 5: Strain gauge data versus F_y and M_x/a as well as a line fitted through the F_y data. F_y and M_x/a are in accordance to each other.

The insulated leads of the strain gauges are glued inside the hole at the bottom of the post and therefore the length of the lead wires can vary depending on the point on the insulated lead wires that is glued to the post. The length of exposed lead wire on the prototypes is 4.3 mm for the slotted post and 4.4 mm for the normal post.

The amount of movement in the vertical direction was tested by inserting a post in a hole of a board made of 1.7 mm thick formply and fastening a nut on the part of the post that sticks out of the formply. The post was unable to move in the vertical direction and therefore the movement in the vertical direction is 0 mm.

The amount of levels of vertical staggering and the extended rod length can be checked on the technical drawings. Both post A and post B have 5 levels of vertical staggering and the bottom flat face on post B is at the same height as the top flat face on post A. The flat faces are 10 mm apart so that moving the turbine disk to a neighbouring flat face results in 10 m vertical staggering when a life-size scale turbine disk with diameter $D = 100$ m or a model turbine disk with diameter $D_m = 10$ mm is used. The extended rod length when the turbine disk is positioned at the bottom flat face of either post can be calculated through some simple geometry and is 0.36 mm.

1.3.4 Conclusion and discussion

One of the two most import requirements is met with the target value: 5 different levels of vertical staggering are met when a model turbine disk with $D_m = 10$ mm or equivalently a turbine disk $D = 100$ m is used. Also, the length of the exposed leads (4.4 and 4.3 mm) is within the target value of 5 mm and the movement in the vertical direction is the target value of 0 mm. The increase in strain gauge signal is 27% higher for a post with a slot compared to a post without a slot and is within the marginal value (20%) but does not meet the target value of 30%. The extended rod length (0.36 mm) is well within the marginal value as well. The prototypes are not suitable to use in a scaled down wind farm setup but the final design is satisfactory.

There is still room for improvement even though all requirements are met within their marginal value. The posts can be shortened at the top so that the model turbine disk covers the top of the post completely even when the disk is attached to the lowest flat face while maintaining 5 different levels of vertical staggering. In order to get a better strain gauge signal a different material with a lower Young's modulus can be used.

2 Research

2.1 Introduction

Wake effects are prominent in wind farms and it is of great importance to reduce the wake effects in order to improve the overall performance of a wind farm. One method that has widely been subject to research is horizontal staggering of wind farms [2, 3] while vertical staggering of wind farms has only been studied to some extend. Most studies on vertical staggering are simple analytical wake model studies based on the Jensen model [4] and various optimisation methods [3, 5–8]. Limited reliable experimental reference data on the effect of vertical staggering in large wind farms [9, 10] and advanced numerical simulation data [10, 11] exist. Recently the effect of vertical staggering has been studied using Large Eddy Simulations (LES) by Zhang et al. [12] in which different amounts of vertical staggering were investigated when each odd numbered turbine row consists of lowered turbines while the even turbine rows consist of elevated turbines. They found that the performance of the wind farm increased significantly in the entrance region of the wind farm when vertical staggering is applied compared to a reference case in which the turbines are vertically aligned, i.e in which all turbines have the same hub height. Another study by Zhang and Stevens [13] suggests that elevating the odd turbine rows and lowering the even turbine rows instead and applying vertical staggering improves the performance of a wind farm even more. Figure 6 (a) gives a visualisation of the setups studied by Zhang et al. and Figures 6 (a) and (b) a visualisation of the setups studied by Zhang and Stevens.

The goal of this study is to validate the LES data for the entrance region of the wind farm by Zhang et al. and Zhang and Stevens by means of experiments. This is done by placing 30 scaled-down wind turbines (ratio 1:100) in a wind tunnel that are designed so that vertical staggering can be applied without having to replace each turbine for every setup. See section 1 for details. More details about the experimental setup, such as the incoming flow characteristics, scaling down of the wind turbines, instrumenting the turbine posts and data acqusition, are discussed in section 2.2. Section 2.3 discusses the power production in the entrance region of the scaled-down wind farm and compares the results to LES data from Zhang et al. and Zhang and Stevens. The streamwise velocity profiles are also discussed in section 2.3. This report is concluded with a discussion of the results in section 2.4 and recommendations in section 2.5.

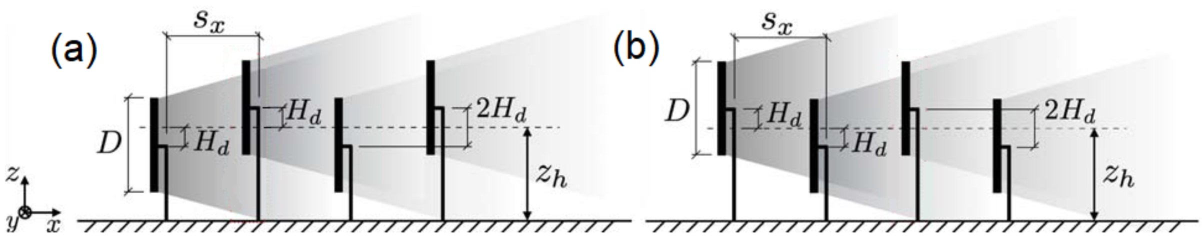

Figure 6: Vertically staggered wind farm configuration (sideview) with (a) the odd turbine rows lowered and (b) the odd turbine rows elevated. The grey gradient patterns behind the turbines show the linearly expanding wakes. The streamwise spacing s_x is made non-dimensional by the turbine rotor diameter D. H_d indicates the height difference relative to the average turbine hub height z_h. Note that the difference in height between two consecutive turbines is $2H_d$. Adapted from [13].

2.2 Experimental setup

In this study, experiments are conducted in the Boundary Layer Wind Tunnel (BLWT) at the School of Civil Engineering within the University of Sydney. It facilitates a test section of 2.5 m wide and 2 m high with a working section of 19 m long and it is a closed loop facility. A turntable that can rotate 360 degrees is installed in the floor in the last 6 m of the test section. A 250 kW fan is installed to drive the flow and freestream velocities of about 27 m/s can be generated in its current configuration. Before entering the test section, the flow generated by the fan passes through a flow straightener, a number of fine mesh screens and a contraction (area ratio 4.5:1). The boundary layer thickness of the developed flow at the entrance of the test section is $\delta \approx 0.31$ m.

In this study formply floorboards with a thickness of 17 mm are used to position the scaled down wind turbine in the wind tunnel. The floorboards are elevated from the wind tunnel floor by 6 mm. In order to create the best flow transition from the wind tunnel floor to the floorboards, a ramp made out of two pieces of formply (1200 mm x 2400 mm) with the long ends side by side is used making it a 2400 mm x 2400 mm ramp. This alters the incoming flow. A wind profile measurement was taken using at Cobra Probe from TFI, Australia, at the position of the first turbine row for two different wind speeds and the results can be seen in Figure 7. Details about velocity profile measurements will be discussed later in this section. The grey fitted line is based on a logarithmic relation between the velocity and the vertical position [14, 15] although some prefer to use the relation based on a power law instead [16–20]:

$$\frac{u}{u_*} = \frac{1}{\kappa} \ln\left(\frac{z}{z_0}\right), \tag{1}$$

in which u is the velocity, z the height, u_* the shear velocity, z_0 the surface roughness length and κ the Von Kármán constant (~ 0.4 for air). u_* and z_0 can be estimated by regressing $\ln z$ against u. Equation 1 becomes

$$\ln z = mu + c. \tag{2}$$

u_* and z_0 can now be estimated by

$$\begin{aligned} u_* &= \kappa/m \\ z_0 &= \exp(c) \end{aligned} \tag{3}$$

For the high speed case ($U_{\text{freestream}} \approx 19.5$ m/s), $u_* = 0.58$ and $z_0 = 0.014$ while for the low speed case ($U_{\text{freestream}} \approx 10$ m/s, $u_* = 0.49$ and $z_0 = 0.030$, which confirms that the method discussed above is just an estimate of the shear velocity and roughness length. The surface roughness length found for both cases resemble water surfaces ($z_0 \approx 0.2$) [21] which is desired since wind farms of the proportion of the wind farm studied in this study are mainly build off-shore. The reference velocity is obtained by a dual-sensor probe from Dantec and the freestream velocity is measured using a pitot tube about half a meter away from the ceiling of the wind tunnel and was connected to a Halstrup pressure transmitter. By fitting Equation 1 to the data from the Cobra Probe an estimation of the effect of the ramp on the boundary layer thickness can be made. The boundary layer thickness at low inflow speed ($\delta \approx 300mm$) is similar to the boundary layer thickness of the test section without obstacles ($\delta \approx 310$ mm), but the boundary layer thickness at high inflow speed ($\delta \approx 380$ mm) is significantly higher than that of the test section without obstacles. Figure 8a shows the velocity profile measured by the Cobra probe and the fitted line according to Equation 1 on a logarithmic X-scale such that it is easier to compare with Figure 2b from Zhang and Stevens. It is evident that the incoming velocity profile in this study is higher compared to the velocity profile in Zhang and Stevens. The turbulence intensity as obtained from the Cobra probe data can be seen in Figure 8b. The fitted line through the data points is based on the logarithmic law for the mean and the variance and is of the form [13]

$$TI = (u')^2/(u^*)^2 = B_1 - A_1 \ln(z). \tag{4}$$

Typically, the values for A_1 and B_1 are $A_1 \approx 1.25$ and $B1 \approx 1.5 - 2.1$ [22]. However, for the data found for the high speed inflow, $B_1 \approx 1.6$ and $A_1 \approx 2.1$ which means that B_1 is in the typical range but A_1 is significantly higher. For the low speed case, $A_1 \approx 2.3$ which is not even close to the typical value, and $B_1 \approx 1.2$ which is outside the typical value range for B_1. In both cases the slope A_1 is higher and since there is a minus sign in front of A_1 in Equation 4, the turbulence intensity decreases less with lower z. This explains why the overall turbulence intensity levels are lower as compared to Zhang and Stevens.

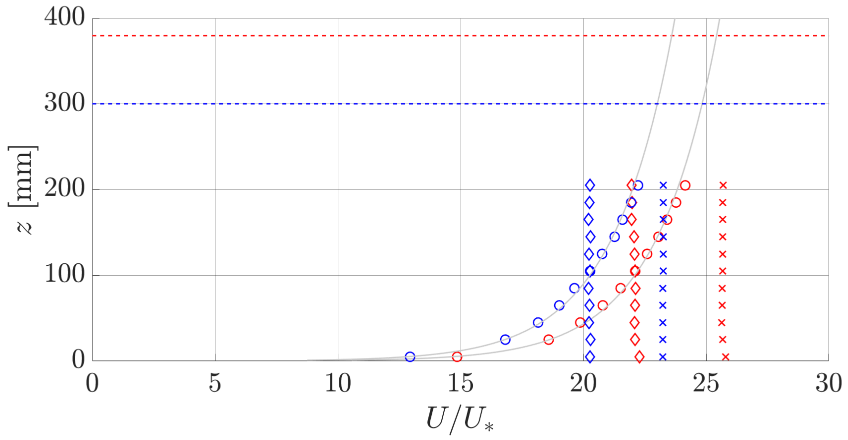

Figure 7: Velocity profiles at $x/D = 0$ for two different wind speeds (red = high speed, blue = low speed). The freestream velocity, reference velocity and velocity measured by the cobra probe are indicated by the crosses, diamonds and circles, respectively. The dashed lines indicate the boundary layer thickness ($u(\delta) = 0.99\ u_{freestream}$) and the grey lines represent the theoretical relation based on Equation 1. See the text for an explanation on obtaining u_* and z_0.

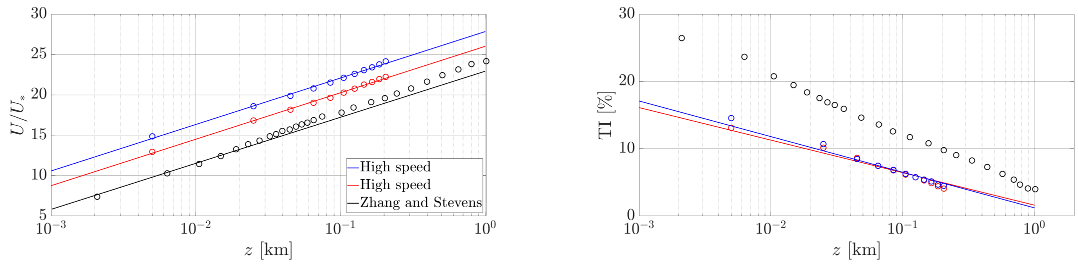

(a) (b)

Figure 8: (a) Inflow velocity profile and (b) 1-D turbulence intensity of the flow at two different inflow speeds and data from Zhang et al. The circles represent the data acquired by the Cobra probe and the solid lines are the fitted lines according to the theory, which is equation 1 for (a) and equation 4 for (b).

Scaling down the wind turbines means that the wind turbine blades have to be scaled down as well while maintaining the correct characterisation of the wake structure [23]. Many possible approaches have been suggested by previous studies based on geometric scaling [13, 24–35], but with the intention of potentially installing numerous rows of wind turbines in the wind tunnel and being able to build and operate the majority of them in mind, scaled rotating wind turbine models are impractical. Also, large scale differences caused by the scaled rotating wind turbine models makes achieving perfect flow similarities impossible. Therefore, a porous disk is used to model the turbines instead. A porous disk model generates small-scale turbulence in the wake close to the disk because of the dissipation of energy instead of extracting energy from the flow directly. Previous studies have proven that porous disks can create approximately similar wake effects as turbine blades in wind tunnels [23, 36–38] and as actuator disks in numerical simulations [15, 39–43]. A porous disk suffices for this study since the interest in this study is not in near wake effects of the turbines but in the power output of a wind farm consisting of multiple wind turbines and thus focuses on physical phenomena present on length and timescales that are larger than the near wake effects of a turbine blade. The porous disks used in this study are made of steel and have a diameter D of 0.1 m, thickness of 0.003 m and a porosity of 58%.

The wind turbine posts are made of perspex with a diameter of 12 mm, a Young's modulus of 3.2 GPa and have a height of 131 mm or 171 mm. Refer to 1 for detailed description of the turbine posts. In order to measure the strain instantaneously the posts are instrumented with a pair of GFLA-3-70-3LJC strain gauges with a strain resistance of 118.7 ± 0.5 and gauge factor $2.10 \pm 0.1\%$ to form a half bridge as discussed in section 1.1.2. A static calibration is done on each individual post using a multi-axis load cell (JR3 30AE12A4, 100N) that measures the forces and moments along three orthogonal axes. This is done by mounting the post in the JR3 and applying known weights after positioning it horizontally and taring the strain gauge signal and the JR3 signals to test the response of the strain gauge signals while also measuring the forces and moments from the load cell under loading of a known weight. The strain signal is acquired with a National Instruments Cdaq-9174 system with an NI-9239 module with a sampling rate of 100 kS/s/ch and 24-bit resolution and the JR3 signal is acquired with two NI-9215 16-bit modules with a sampling rate of 100 kS/s/ch. Since the amount of strain is directly and linearly related to the moment around the location of the strain gauges on the post, and since the strain is expected to be 0 when no load is applied, the slope a in the relation $\varepsilon = aM$ can be calculated, in which ε is the strain M is the moment. Any strain can now be converted to a moment. If the assumption is made that the point on which the force acts due to the loading of the wind on the turbine disk is the position of the turbine disk on the post, the arm can be calculated to determine the corresponding thrust force. An example of such a strain-force relationship can be seen in Figure 9. This thrust force can in turn be converted to an average velocity on the disk through the relation $F = \rho \langle U \rangle^2 C_T A/2$, where $A = \pi D^2/4$ is the span of the turbine disk area. Finally, the power output can be calculated through $P = \rho \langle U \rangle^3 C_p A$. Since in this study identical turbine disks are used in all setups and the results are normalised, the values of C_T and C_p are not relevant when the power output is calculated. See section 2.3 for more details. However, a previous study [44] has shown that the thrust coefficient of the turbine disks used in this study varied between 0.75 and 0.85 depending on the wind speed. These thrust coefficient values are within the thrust coefficient values reported for commercial full-scale wind turbines [45, 46] and thus represent full-scale wind turbines.

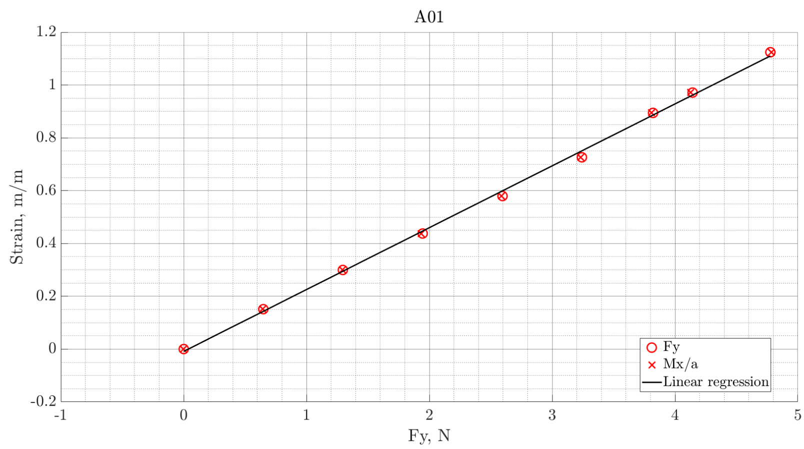

Figure 9: Typical strain response due to a load at the end of the post. The figure shows the downward force F_y and the force reconstructed from the moment around x, M_x, from the JR3 signals. The arm a is calculated by determining the ratio $\langle F_y/M_x \rangle$, where $\langle . \rangle$ indicates the mean over all data points.

The purpose of this study is to verify the numerical simulations done by Zhang et al. [12] and Zhang and Stevens [13] on the effect of vertically staggered wind farms in the entrance region. Most parameters are the same although some parameters are slightly different such as the streamwise and the spanwise spacing, s_x and s_y, respectively. The power output will be measured for fifteen different setups and the velocity profile at $x/D = 1$ will be taken for six of these setups. A summary of the wind farm configurations can be found in Table 2. During each experiment, only the three middles columns are strain gauged and the two outer columns of wind turbines act purely as boundary layer development. The velocity profile measurements will be conducted behind row 2 and row 3 of case $a0$, $a4$, $b0$, $b4$, $c0$ and $c4$ i.e. the reference vertically aligned setup and maximum staggering ($H_d = 40$) when the first row of wind turbines consists of short turbines at high speed wind flow and the reference setup and maximum staggering when the first row of wind turbines consists of tall turbine at high speed and low speed wind flow. During the power output measurements, a TMR-211 data logger records the data from the strain gauges at a sample rate of 2048 Hz. The velocity flow measurements are taken by a Cobra Probe from TFI which measures the flow velocity in three directions at a sample rate of 4096 Hz. The Cobra probe is attached to a traverse with a resolution of 1 mm that enables the positioning of the Cobra probe to the desired location.

2.3 Results

2.3.1 Power output

In the left column of Figure 10 the row averaged turbine power output, normalised by the row averaged power output of the first row of the corresponding reference setup, is shown as a function of the turbine row for all cases. The results are averaged over time and averaged over the three middle turbines of the row. The data used to obtain the average values is within 15% of the average value. This uncertainty is due to the power output of the middle column of wind turbines being lower in general than the power output of the two neighbouring columns. This difference in power output between the columns is most prominent for cases $b0 - b4$ and $c0 - c4$, i.e. the cases in which the odd rows of the wind farm consist of tall turbine posts, although no correlation between the value of H_d and the power output is noticeable.

The power output of the first turbine row drops as H_d increases when the odd rows consist of short turbines, see Figure 10a, while the power production of the second row increases as H_d increases. This is as expected since a short wind turbine will capture lower velocities on average due to the logarithmic mean velocity profile in the boundary layer compared to a tall wind turbine. The taller wind turbines in the second row, however, are exposed to a greater portion of the incoming undisturbed wind of higher velocity and can hence produce more power. Due to the vertical staggering, the second row of turbines is placed further out of the wake of the preceding turbine when H_d increases as well, thus resulting in a higher power output. The power output of the first two rows combined can be significantly higher compared to the reference aligned wind farm, see Figure 10b, which shows the relative cumulative power output up until a row. This means that vertical staggering greatly improves the power output of the first part of the entrance region of the wind farm. Figure 10a also shows that the power production of the even rows (tall turbines) is higher than the power production of the odd rows (short turbines). This zigzag pattern occurs due to the reason given above, namely that the taller turbines have better access to the undisturbed atmospheric flow due to the preceding turbines being lower. The power gained by elevating the turbines in the even rows is higher than the loss of power by lowering the turbines in the odd rows. This could be an indication that wakes inside the wind farm recover rapidly due to the downward vertical kinetic energy flux. Streamwise velocity profile measurements will have to be taken at various distances behind the wind turbines in order to confirm this hypothesis. Figure 10b suggests that the power output of the entrance of a wind farm can be as high as 121 % compared to a vertically aligned wind farm.

The power output of the first turbine row increases slightly as H_d increases except for $H_d = 10$, but

Table 2: Summary of the fifteen different cases. All cases have the same turbine hub height $z_h = 100$ m, turbine diameter $D = 100$ m, height difference relative to the hub height $H_d = 0,\ 10,\ 20,\ 30\ 40$ m, number of turbines in the streamwise and spanwise direction $N_x \times N_y = 6 \times 5$, streamwise spacing $s_x = 5$ and spanwise spacing $s_y = 5$. Definitions of the parameters can be found in Figure 6.

Case Name	Odd turbine rows lowered/elevated	Freestream velocity [m/s]	Reference case
$a0$ - $a4$	Lowered	19.5	$a0$
$b0$ - $b4$	Elevated	19.5	$b0$
$c0$ - $c4$	Elevated	11.0	$c0$

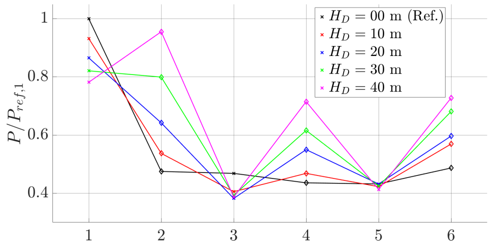

(a) Cases $a0$ - $a4$ (Short turbines in odd rows, high speed)

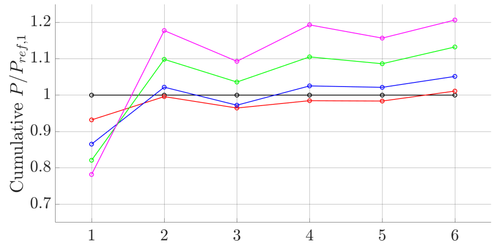

(b) Cases $a0$ - $a4$ (Short turbines in odd rows, high speed)

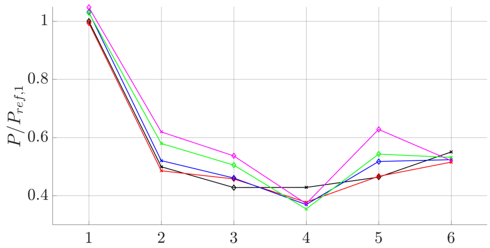

(c) Cases $b0$ - $b4$ (Tall turbines in odd rows, high speed)

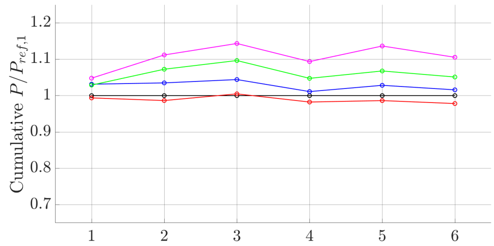

(d) Cases $b0$ - $b4$ (Tall turbines in odd rows, high speed)

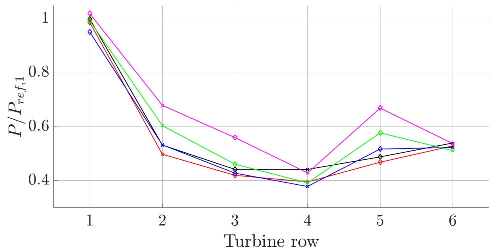

(e) Cases $c0$ - $c4$ (Tall turbines in odd rows, low speed)

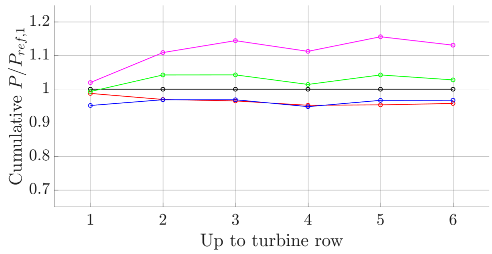

(f) Cases $c0$ - $c4$ (Tall turbines in odd rows, low speed)

Figure 10: (Left) Normalised power output $P/P_{ref,1}$, in which $P_{ref,1}$ is the average power output of the first row of turbines of the reference case, as a function of the downstream position. The crosses represent a row of short turbine posts while the diamonds represent a row of tall turbine posts. (Right) Relative cumulative power output: the ratio of the power production of the vertically staggered wind farm up to the row indicated on the x-axis divided by the power production of the reference alined wind farm.

this can be a cause of statistical errors in the data. Even the power output of the second row increases with increasing H_d, see Figure 10c. This suggests that clearance of the small turbine in the second row from the wake of the preceding tall turbine makes up for the lower incoming velocity due to the incoming logarithmic profile. It is not until the fourth turbine row that vertically staggered wind farms have a disadvantage over a vertically aligned wind farm after which the zigzag pattern appears just like for the cases $a0 - a4$. Figure 10d shows that the power output in the entrance region is always higher than the reference vertically aligned case when $H_d > 10$.

The pattern of the power output of the cases where a tall turbine is placed in the odd numbered rows and short turbines in the even numbered rows with a lower incoming wind speed is similar to the pattern of the high speed inflow case, see Figure 10e. The total power output of wind farm is higher than the reference aligned wind farm when $H_d = 30$ or $H_d = 40$, but smaller amounts of vertical staggering are less beneficial than the reference wind farm. On the other hand, the total power output of a wind farm in which $H_d = 40$ generates more power at low incoming wind speed compared to the reference case at low speed than the same wind farm with high incoming wind speed. Vertically staggered wind farms with large H_d thus seem more effective at low wind speeds compared to the vertically aligned wind farm.

As a check to whether the power output differs between a tall turbine and a small turbine due to mechanical effects, the reference cases $a0$ and $b0$ are plotted in Figure 11. It can be observed in Figure 11a that the power output of the short turbine posts in each turbine row is within a few percents of the tall turbine post. Figure 11b confirms that the total power output of six turbine rows comibned for the two cases is almost the same and that differences in short and tall turbines can be neglected.

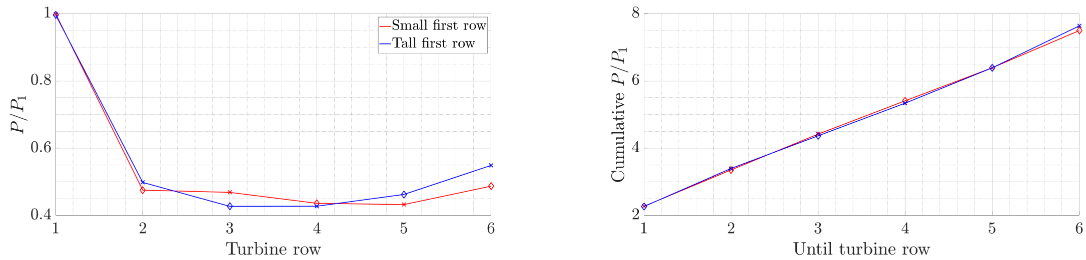

(a) *(b)*

Figure 11: Comparison between the power production of cases $a0$ and $b0$ to test the difference in post response between a tall and short turbine post. The diamonds indicate tall turbine posts and the crosses indicate short turbine posts.

Figure 12a presents a comparison between the reference experimental case at high incoming wind speed (case $a0$), the power output of maximum vertical staggering when (a) the odd turbine rows are lowered with high wind speed inflow, (b) the odd turbine rows are elevated with high wind speed inflow, (c) the odd turbine rows are elevated with low wind speed inflow, as well as the corresponding LES results from Zhang et al. and Zhang and Stevens. When comparing the reference cases in the figure, the power output of the first three rows are marginally similar while the power output of the last three turbines of the experiments is found to be lower than the numerical results even though the incoming wind speed is higher in the experiments. When comparing the cases where the odd turbine rows are lowered, the power production of the experiments is higher than those of the numerical results, as expected because of the higher incoming wind speed in the experiments. Figure 12b confirms that the total power output of the experimental wind farm when the odd turbine rows are lowered is higher than the corresponding numerical case. When comparing the power production of the cases where the odd turbine rows are elevated the experiments produce less power in the first and third row compared to the LES case at high incoming flow speed and at low incoming flow speed. However, this loss is made up for in the last three rows and both the high speed and low speed incoming flow cases produce roughly the same amount of power over the first six turbine rows combined. Surprisingly the experiments suggest that a wind farm in which the odd turbine rows are lowered produce more power in the entrance region compared to a wind farm in which the odd turbine rows are elevated which contradicts to the numerical results from Zhang et al. and Zhang and Stevens.

2.3.2 Streamwise velocity profiles

Figure 13 shows the streamwise velocity profiles normalised by the shear velocity u_* at position $x/D = 1$ behind row 2 (left column) and behind row 3 (right column). Qualitatively the experiments follow the profile of the numerical study, i.e. there is a velocity deficit at the vertical positions where a turbine is present. For the cases where the streamwise velocity profile is taken on a short turbine on which maximum staggering is applied, see the magenta lines in Figures 13b, 13c and 13e, a difference between the experiments and the LES can be noted. Whereas in the other figures the normalised velocity increases as z increases after the turbine hub height has been passed, those cases show that the velocity remains approximately the same for the points of the top of the turbine disk and its subsequent higher point. This can be caused by the extended rod behind the turbine disk which causes an extra

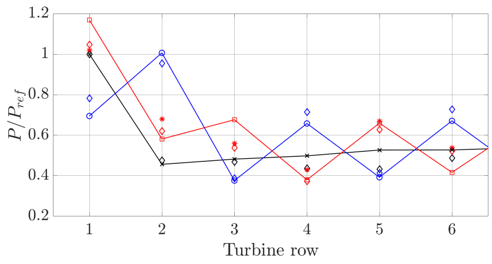

(a)

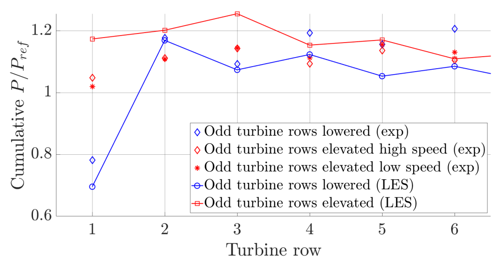

(b)

Figure 12: Comparison between the experimental data and the LES data from Zhang et al. and Zhang and Stevens. The black line in the left figure is the reference LES case and the black diamonds are the reference experimental case at high speed wind inflow.

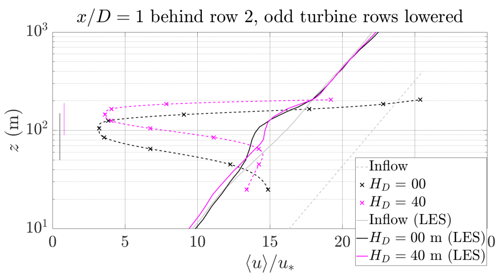

(a) Cases $a0$ / $a4$ (Short turbines in odd rows, high speed)

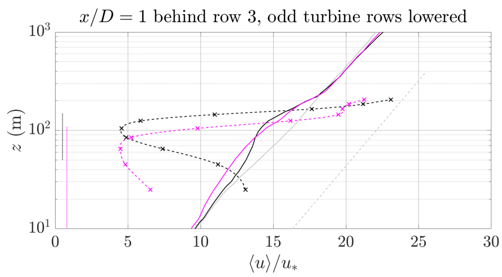

(b) Cases $a0$ / $a4$ (Short turbines in odd rows, high speed)

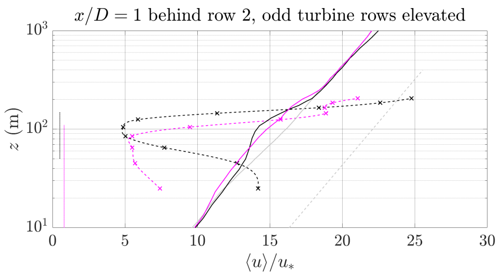

(c) Cases $b0$ / $b4$ (Tall turbines in odd rows, high speed)

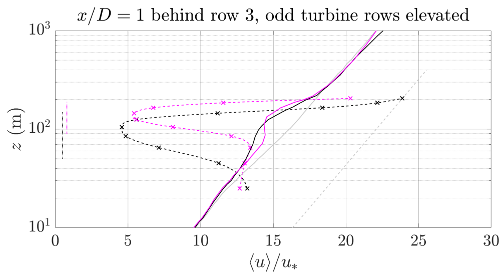

(d) Cases $b0$ / $b4$ (Tall turbines in odd rows, high speed)

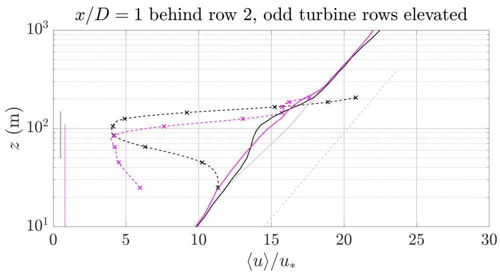

(e) Cases $c0$ / $c4$ (Tall turbines in odd rows, low speed)

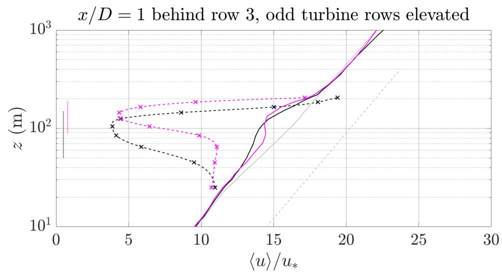

(f) Cases $c0$ / $c4$ (Tall turbines in odd rows, low speed)

Figure 13: Streamwise velocity profiles for each case. The left column of figures shows the velocity profiles behind row 2 and the right column of figures the velocity profiles behind row 3. The profiles are taken behind the wind turbine in the middle column. The corresponding LES results from Zhang and Stevens are included in the figures.

drag. The velocity profiles behind row 3 (Figures 13d, 13f) show that subsequent turbines are not affected by this. Quantitatively, the drop of the normalised velocity is significantly higher in all the experimental cases compared to the corresponding LES cases. This is due to the high turbulence intensity behind the turbine disks as is illustrated in Figure 14. The figures show that the turbulence intensity can reach up to 41% which is considerably higher than the turbulence intensities reported by the literature for $x/D = 1$ behind a free standing single wind turbine [44] and further downstream of a free standing single wind turbine [44, 47]. The wake recovery rate, however, must be high considering the power production of the wind farms in this study are similar to the power output of the numerical studies by Zhang et al. and Zhang and Stevens.

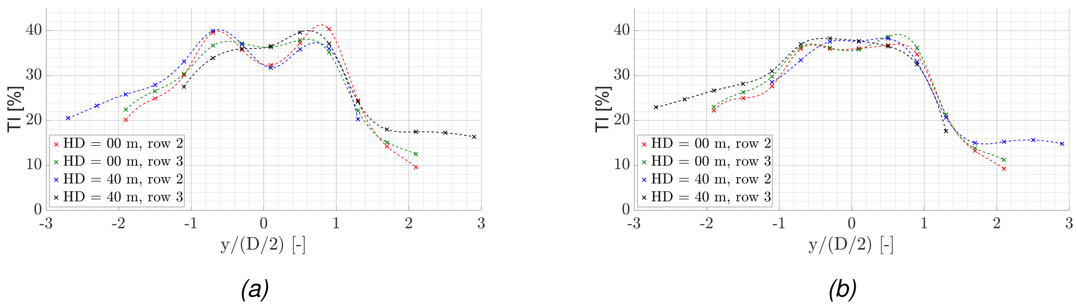

Figure 14: Turbulence intensity in three dimensions as a function of the vertical position centered at the hub height and normalised by the turbine disk radius. (a) odd turbine rows are lowered, (b) odd turbine rows are elevated (high speed incoming flow).

2.4 Conclusion and discussion

In this work, the effect of vertical staggering in the entrance region of a large wind farm is studied using the Boundary Layer Wind Tunnel in the School of Civil Engineering within the University of Sydney. Fifteen different setups were considered (see Table 2) in which the key parameters were the same such as the mean hub height z_h, turbine diameter D, number of turbines in the streamwise and spanwise direction N_x and N_y and the streamwise and spanwise spacing s_x and s_y. Parameters that varied were whether the odd turbine rows are lowered or elevated and the incoming freestream velocity. The experiments show that the power production of a wind farm in which maximum staggering is applied ($H_d = 40$ m) is higher when the odd turbine rows are lowered than when the odd turbine rows are elevated which conflicts with the results of the numerical studies by Zhang et al. [12] and Zhang and Stevens [13]. Also, the power production of a wind farm in which the odd turbine rows are lowered is higher than expected from the LES study while the power production of a wind farm in which the odd turbine rows are elevated is roughly the same compared to the LES study. It has to be noted though that the streamwise spacing, spanwise spacing and the incoming flow speed was different in the numerical study compared to this study. The effect of vertical staggering in the entrance region is more beneficial for smaller streamwise turbine spacing [13] so higher power production for the experiments compared to the LES is expected. Also the data presented in this work is within an error margin of 15% which is inaccurate and by redoing the experiments, slightly different outcomes are likely to be found.

The streamwise velocity profiles from the experiments are qualitatively similar to the velocity profiles of the LES except for the cases in which maximum vertical staggering is applied on a short post so that a part of the post is present behind the turbine disk. However, this does not affect the power output of the wind turbine and any subsequent wind turbines. Quantitatively the velocity deficit is much higher in the experiments compared to the LES. This is due to the high level of turbulence (up to 41%) directly behind the wind turbines but the wake recovery rate is high as well so that the mean incoming velocity at subsequent turbines is relatively unaffected by the turbulence.

2.5 Recommendations

The conclusions reached here are subject to limitations in the setup and in the flow conditions and can be improved in future experiments. The alignment of the floorboards on the wind tunnel floor relative to the flow was not perfect but it was kept constant throughout all experiments. In order to see the development of the flow behind the wind turbines, wake measurements such as normalised streamwise velocity and turbulence intensity can be taken at more positions downstream, e.g. at $x/D = 1, 3$ and 5, and should be compared against previous experimental results of rotating and non-rotating turbine models. The turbulence intensity in each direction should be looked at as well and can give more insight in the wake recover. Also the difference in the power output between the middle column and its neighbouring columns should be investigated by swapping around the turbines between the middle column and a neighbouring column. Furthermore a dynamic calibration should be done in order to investigate the natural frequency of the posts and to investigate the influence of turbulence on the strain gauge output. Validation of the strain gauge data and the velocity profile measurements can be done by looking at the probability densities and by filtering the signals to give more accurate results. Furthermore, the LES studies only model the turbine disks and do not model the turbine posts. The effect of the turbine posts can also be investigated. Also, the strain gauge signal did not return to zero after unloading the turbines which might have caused the signal to drift. However, this effect is minor and should not influence the strain gauge signal by a significant amount.

References

[1] T. R. Kuphalt, *Lessons in Electric Circuits: Volume I - DC*, vol. 1. 5th ed., Oct. 2006.

[2] R. J. Stevens and C. Meneveau, "Flow Structure and Turbulence in Wind Farms," *Annual Review of Fluid Mechanics*, vol. 49, no. 1, pp. 311–339, 2017.

[3] J. F. Herbert-Acero, O. Probst, P.-E. Réthoré, G. C. Larsen, and K. K. Castillo-Villar, "A Review of Methodological Approaches for the Design and Optimization of Wind Farms," *Energies*, vol. 7, pp. 6930–7016, 2014.

[4] N. Jensen, *A note on wind generator interaction*. Risø National Laboratory, 1983.

[5] Y. Chen, H. Li, K. Jin, and Q. Song, "Wind farm layout optimization using genetic algorithm with different hub height wind turbines," *Energy Conversion and Management*, vol. 70, pp. 56–65, June 2013.

[6] K. Chen, M. X. Song, X. Zhang, and S. F. Wang, "Wind turbine layout optimization with multiple hub height wind turbines using greedy algorithm," *Renewable Energy*, vol. 96, pp. 676–686, Oct. 2016.

[7] B. DuPont, J. Cagan, and P. Moriarty, "An advanced modeling system for optimization of wind farm layout and wind turbine sizing using a multi-level extended pattern search algorithm," *Energy*, vol. 106, pp. 802–814, July 2016.

[8] A. Vasel-Be-Hagh and C. L. Archer, "Wind farm hub height optimization," *Applied Energy*, vol. 195, pp. 905–921, June 2017.

[9] L. P. Chamorro Chavez, N. Tobin, R. E. A. Arndt, and F. Sotiropoulos, "Variable-sized wind turbines are a possibility for wind farm optimization," *Wind Energy*, vol. 17, no. 10, pp. 1483–1494, 2014.

[10] S. Xie, C. L. Archer, N. Ghaisas, and C. Meneveau, "Benefits of collocating vertical-axis and horizontal-axis wind turbines in large wind farms," *Wind Energy*, vol. 20, pp. 45–62, Jan. 2017.

[11] L. Wang, A. C. C. Tan, M. Cholette, and Y. Gu, "Comparison of the effectiveness of analytical wake models for wind farm with constant and variable hub heights," *Energy Conversion and Management*, vol. 124, pp. 189–202, Sept. 2016.

[12] M. Zhang, M. G. Arendshorst, and R. J. A. M. Stevens, "Large eddy simulations of the effect of vertical staggering in large wind farms," *Wind Energy*, vol. 22, no. 2, pp. 189–204, 2019.

[13] M. Zhang and R. J. Stevens, "Exploring a better turbine layout in vertically staggered wind farms," *Journal of Physics: Conference Series*, vol. 1037, p. 072041, June 2018.

[14] N. E. Bergeron and A. D. Abrahams, "Estimating shear velocity and roughness length from velocity profiles," *Water Resources Research*, vol. 28, no. 8, pp. 2155–2158, 1992.

[15] R. J. A. M. Stevens, L. A. Martínez-Tossas, and C. Meneveau, "Comparison of wind farm large eddy simulations using actuator disk and actuator line models with wind tunnel experiments," *Renewable Energy*, vol. 116, pp. 470–478, Feb. 2018.

[16] G. I. Barenblatt and V. M. Prostokishin, "Scaling laws for fully developed turbulent shear flows. Part 2. Processing of experimental data," *Journal of Fluid Mechanics*, vol. 248, pp. 521–529, 1993. bibtex*[publisher=Cambridge University Press].

[17] G. I. Barenblatt, “Scaling laws for fully developed turbulent shear flows. Part 1. Basic hypotheses and analysis,” *Journal of Fluid Mechanics*, vol. 248, pp. 513–520, 1993. bibtex*[publisher=Cambridge University Press].

[18] G. I. Barenblatt and N. Goldenfeld, “Does fully developed turbulence exist? Reynolds number independence versus asymptotic covariance,” *Physics of Fluids*, vol. 7, no. 12, pp. 3078–3082, 1995.

[19] G. I. Barenblatt and A. J. Chorin, “A mathematical model for the scaling of turbulence,” *Proceedings of the National Academy of Sciences of the United States of America*, vol. 101, p. 15023, Oct. 2004.

[20] B. Cipra, “A New Theory of Turbulence Causes a Stir Among Experts,” *Science*, vol. 272, p. 951, May 1996.

[21] Standards Australia, “Structural design actions—Wind actions—Commentary,” tech. rep., Supplement to AS/NZS 1170.2:2002, Standards Australia, NSW, 2002.

[22] R. J. A. M. Stevens, L. A. Martínez-Tossas, and C. Meneveau, “Comparison of wind farm large eddy simulations using actuator disk and actuator line models with wind tunnel experiments,” *Renewable Energy*, vol. 116, pp. 470–478, Feb. 2018.

[23] R. Theunissen, P. Housley, C. B. Allen, and C. Carey, “Experimental verification of computational predictions in power generation variation with layout of offshore wind farms,” Oct. 2015.

[24] P. R. Ebert and D. H. Wood, “The near wake of a model horizontal-axis wind turbine—I. Experimental arrangements and initial results,” *Renewable Energy*, vol. 12, pp. 225–243, Nov. 1997.

[25] J. Whale, C. G. Anderson, R. Bareiss, and S. Wagner, “An experimental and numerical study of the vortex structure in the wake of a wind turbine,” *Journal of Wind Engineering and Industrial Aerodynamics*, vol. 84, pp. 1–21, Jan. 2000.

[26] D. Medici and P. H. Alfredsson, “Measurements on a wind turbine wake: 3d effects and bluff body vortex shedding,” *Wind Energy*, vol. 9, no. 3, pp. 219–236, 2006.

[27] J. Lebron, R. B. Cal, H.-S. Kang, L. Castillo, C. Meneveau, and P. D Student, “Interaction Between a Wind Turbine Array and a Turbulent Boundary Layer,” *11th Americas Conference on Wind Engineering*, 2010.

[28] L. Chamorro and F. Porté-Agel, “Turbulent Flow Inside and Above a Wind Farm: A Wind-Tunnel Study,” *Energies*, vol. 4, pp. 1916–1936, 2011.

[29] R. B. Cal, J. A. Lebrón, L. O. Castillo, H. S. Kang, and C. Meneveau, “Experimental study of the horizontally averaged flow structure in a model wind-turbine array boundary layer,” 2010.

[30] Y. Odemark, “Wakes behind wind turbines - Studies on tip vortex evolution and stability,” no. 2012:06, pp. vi, 78, 2012. QC 20120504 bibtex*[institution=KTH, Mechanics].

[31] L. Lignarolo, D. Ragni, C. J. Simao Ferreira, and G. J. W. van Bussel, “Wind turbine and actuator disc wake: Two experimental campaigns,” *Proceedings of the 14th International Conference on Wind Engineering, ICWE14, Porto Alegre (Brasil), June 21-26, 2015*, 2015.

[32] B. Dou, M. Guala, P. Zeng, and L. Lei, “Experimental investigation of the power performance of a minimal wind turbine array in an atmospheric boundary layer wind tunnel,” *Energy Conversion and Management*, vol. 196, pp. 906–919, Sept. 2019.

[33] L. E. M. Lignarolo, D. Ragni, C. Krishnaswami, Q. Chen, C. J. Simão Ferreira, and G. J. W. van Bussel, “Experimental analysis of the wake of a horizontal-axis wind-turbine model,” *Renewable Energy*, vol. 70, pp. 31–46, Oct. 2014.

[34] H. S. Kang and C. Meneveau, "Direct mechanical torque sensor for model wind turbines," *Measurement Science and Technology*, vol. 21, p. 105206, Sept. 2010. bibtex*[publisher=IOP Publishing].

[35] J. Bartl, F. Pierella, and L. Sætrana, "Wake Measurements Behind an Array of Two Model Wind Turbines," *Energy Procedia*, vol. 24, pp. 305–312, Jan. 2012.

[36] L. E. M. Lignarolo, D. Ragni, C. J. S. Ferreira, and G. J. W. van Bussel, "Kinetic energy entrainment in wind turbine and actuator disc wakes: an experimental analysis," *Journal of Physics: Conference Series*, vol. 524, p. 012163, June 2014. bibtex*[publisher=IOP Publishing].

[37] S. Aubrun, S. Loyer, P. E. Hancock, and P. Hayden, "Wind turbine wake properties: Comparison between a non-rotating simplified wind turbine model and a rotating model," *Journal of Wind Engineering and Industrial Aerodynamics*, vol. 120, pp. 1–8, Sept. 2013.

[38] G. España, S. Aubrun, S. Loyer, and P. Devinant, "Spatial study of the wake meandering using modelled wind turbines in a wind tunnel," *Wind Energy*, vol. 14, no. 7, pp. 923–937, 2011.

[39] J. Meyers and C. Meneveau, "Optimal turbine spacing in fully developed wind farm boundary layers," *Wind Energy*, vol. 15, no. 2, pp. 305–317, 2012.

[40] S. De Rijcke, J. Driesen, and J. Meyers, "Power smoothing in large wind farms using optimal control of rotating kinetic energy reserves," *Wind Energy*, vol. 18, no. 10, pp. 1777–1791, 2015.

[41] Y.-T. Wu and F. Porté-Agel, "Large-Eddy Simulation of Wind-Turbine Wakes: Evaluation of Turbine Parametrisations," *Boundary-Layer Meteorology*, vol. 138, pp. 345–366, Mar. 2011. bibtex*[day=01].

[42] R. J. A. M. Stevens, J. Graham, and C. Meneveau, "A concurrent precursor inflow method for Large Eddy Simulations and applications to finite length wind farms," *Renewable Energy*, vol. 68, pp. 46–50, Aug. 2014.

[43] R. J. A. M. Stevens and C. Meneveau, "Temporal structure of aggregate power fluctuations in large-eddy simulations of extended wind-farms," *Journal of Renewable and Sustainable Energy*, vol. 6, p. 043102, July 2014. arXiv: 1412.7238.

[44] P. Martinez-Giraldo, K. Talluru, and K. Chauhan, "A wind tunnel study of variability in power output of scaled wind turbine farms," (Torquay, Victoria), pp. 1–6, Australasian Wind Engineering Society, 2018.

[45] F. Porté-Agel, H. Lu, and Y.-T. Wu, "Interaction between Large Wind Farms and the Atmospheric Boundary Layer," *Procedia IUTAM*, vol. 10, pp. 307–318, Jan. 2014.

[46] C. Desmond, J. Murphy, L. Blonk, and W. Haans, "Description of an 8 MW reference wind turbine," *Journal of Physics: Conference Series*, vol. 753, p. 092013, Sept. 2016. bibtex*[publisher=IOP Publishing].

[47] J. Bossuyt, M. F. Howland, C. Meneveau, and J. Meyers, "Measurement of unsteady loading and power output variability in a micro wind farm model in a wind tunnel," *Experiments in Fluids*, vol. 58, p. 1, Dec. 2016.

Tutoring

3.1 Job description

The third part of the internship is a tutoring job for the course *CIVL 3612: Fluid Mechanics*. This course is core subject as part of the four year Bachelor of Engineering Honours (Civil) programme, which means that every student has to pass the course in order to get the degree, and it is taught in the first semester of the third year of studying. In the course, students familiarise themselves with various fundamental topics in fluid mechanics, which are acceleration, conservation of mass and momentum, potential flow, the Navier-Stokes equations and dimensionless analysis. In addition, four different applications will be discussed, which are viscous flow in pipes, flow over immersed bodies, open channel flow and pumps, in which the knowledge from the fundamental topics will be applied to real life situations. During the lectures the fundamental concepts are reviewed and explained by Dr Kapil Chauhan. The weekly tutorials focus on engineering problems in which the students are asked to solve problems by themselves or in groups and can ask help or feedback from the tutors. The students are assigned to a tutorial on either Tuesday or Wednesday and the tutors are assigned to a tutorial on both Tuesday and Wednesday. Each tutorial session will have approximately 60 students in them. The last component of the course consists of laboratory experiments in which pipe flow and open channel flow are discussed. More than 320 students are enrolled for the course during Semester 1 2019.

The team of tutors consists of eight tutors including myself. Each of us is in charge of one of the nine topics mentioned above which we discuss in the weekly Monday meetings. Being in charge of a topic means that during the week that your topic is being discussed you are responsible for the content of the tutorial, and during the meetings we discuss said content. Some topics are discussed for two consecutive weeks, which means that the tutor who is in charge of that topic has to come up with two sets of problems. I am responsible for the tutorial on Conservation of Mass and Momentum (see appendix C) which is discussed in the second week of the tutorials.

As mentioned above, students are asked to come up with a solution to the problems given to them in the 2 hour tutorial sessions based on their gained knowledge from the lectures. There is an allocated time for the students to work on each problem before one of the tutors starts discussing the problem in front of the classroom. Figure 15 gives an impression of what the classroom looks like. The students are seated around so called pods - the black screens in Figure 15 - that will display the horizontal whiteboard which is in the middle of the room - the brown desk in Figure 15 - on which the tutor will write hints and eventually the answers to the problem at a time to their own liking. The big screens above the brown desk display the current problem. While one of the tutors is explaining the problem to the class the other tutors walk around and answer questions that the students have.

3.2 Learning objectives

There are multiple reasons why becoming a tutor is benificial for my academic development. Although it being a valuable addition to my resume, I never considered being a tutor at the University of Twente. I kept thinking to myself: am I confident enough to explain problems in class in front of all the students that do not speak my mother tongue? Am I confident enough to be in a room full of eager students to answer their questions? What if I do not know the answer to their questions? Does that mean I am not smart enough? Do I lose their respect if I do not know how to answer their questions?

These questions popped into my head immediately when Kapil offered me the tutoring job and I started to hestitate if I would be capable to do such a job, but after some time to think about the offer I wanted to take the challenge. After all, the goal of the internship is to work in an unfamiliar working environment and be comfartable after working there for a while, so if I want to be a tutor at some point in my life, my internship is a great time to take the leap and go for it. It would boost my confidence and I would

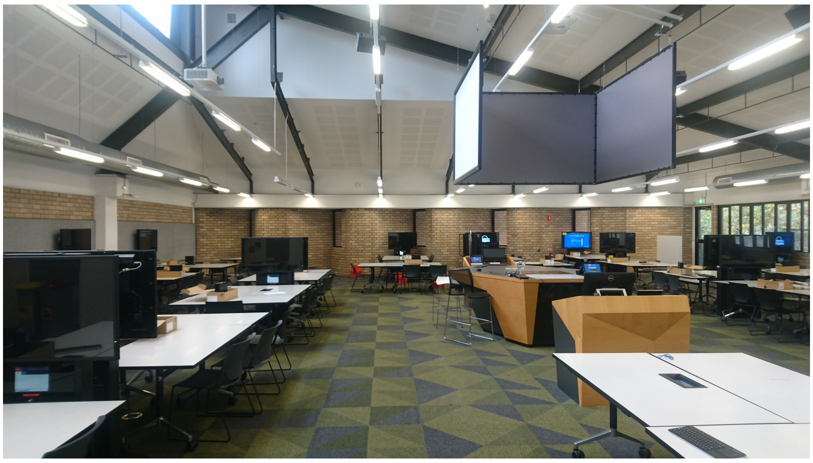

Figure 15: PNR310: one of the rooms in which I am tutoring.

expand my knowledge, gain experience in teaching, be part of a team and also earn some income. The students will also have less hestitation to ask me questions since I am still a student myself which helps me understand their struggles better.

My main learning objective is to be comfortable explaining problems in a foreign language and thereby boost my confidence and communication skills. Furthermore I want to review my knowledge on the various topics that are being discussed in the course, work together closely as a team with the other tutors and get a feeling of what it is like to study at a big international university.

3.3 Self reflection

Since I have worked as a tutor, I have developed a variety of skills that will undoubtedly benefit me in the future, both in my academic development and in my social life. My listening skills have improved incrementally over the past few weeks because of the diversity of the students which sometimes caused difficulties in communication. As the weeks progressed my communication with the students started to improve as I was able to express myself more and more effortless. In the first tutorial sessions I was still nervous. The students were able to pick up on this and tend to get nervous themselves which does not contribute to a good learning environment. Once the nervousness was gone the students started to become calmer, and although the number of students that attend the tutorial sessions dropped, the questions they asked were getting better. The questions changed from basic questions during the first tutorials - which helped me build confidence as I was able to answer them almost instantly - to more advanced questions on the application of certain theory and phenomena. This gradual change in the type of questions also improved my communication skills as I was able to answer the questions without much effort. Interaction between the students and me changed from simple question and simple answer to full discussions about the matter.

The topics that are discussed in this course are taught at an undergraduate level which is comparable to the Bachelor level course in the Netherlands. In my second year of studying Applied Physics I have done a course on fluid mechanics and most of the topics discussed in the tutorials are familiar to me. The main difference between the courses is the application, so based on the same knowledge I have gained a better understanding of the applications of the theory discussed in the course I followed before.

As mentioned before, the team of tutors consists of eight tutors, and although we discussed the content of the tutorials in the Monday meetings, I only worked closely together with three other tutors with whom I lead the tutorial sessions. Since everybody is in charge of explaining one or two of the problems in a tutorial session there is always someone that understands the problem that the student is working on perfectly. This means that whenever you are unable to answer a question you can ask your fellow tutors for a thorough explanation which ensures everyone in the team is a valuable person.

Whereas the tutorials at the University of Twente tend to be focused on working on problems on your own or in groups and ask questions to the tutors whenever you get stuck and only receive the answers to the problems - if at all - after the tutorial, at the University of Sydney students will get the answers regardless of the amount of effort that they put in solving the problem. During the earlier tutorials the students were attending the tutorials and made an effort to try to solve the problems whereas fewer students showed up in later tutorials and were waiting for the answers to appear on the screen. The students are free to do so but in this case completely miss the goal of the tutorial: applying the theory from the lectures to real life engineering problems. Also, everyone is expected to keep up with the pace of the tutors while some students struggle more with the problems than others. This way fewer students will attend the tutorials as well since the tempo is too low for some and too high for others. The upside of this method of teaching is that you rarely get the same questions. If this is the case, however, you tell the tutor who is explaining the current problem to clarify or elaborate on the matter. This is a big advantage over the method generally used at the University of Twente but in my opinion does not outweigh the disadvantages of the method at the University of Sydney. I have learned to appreciate the teaching method of the University of Twente, although the method of the University of Sydney seems to work as well.

Appendix

A. Technical drawings: turbine posts

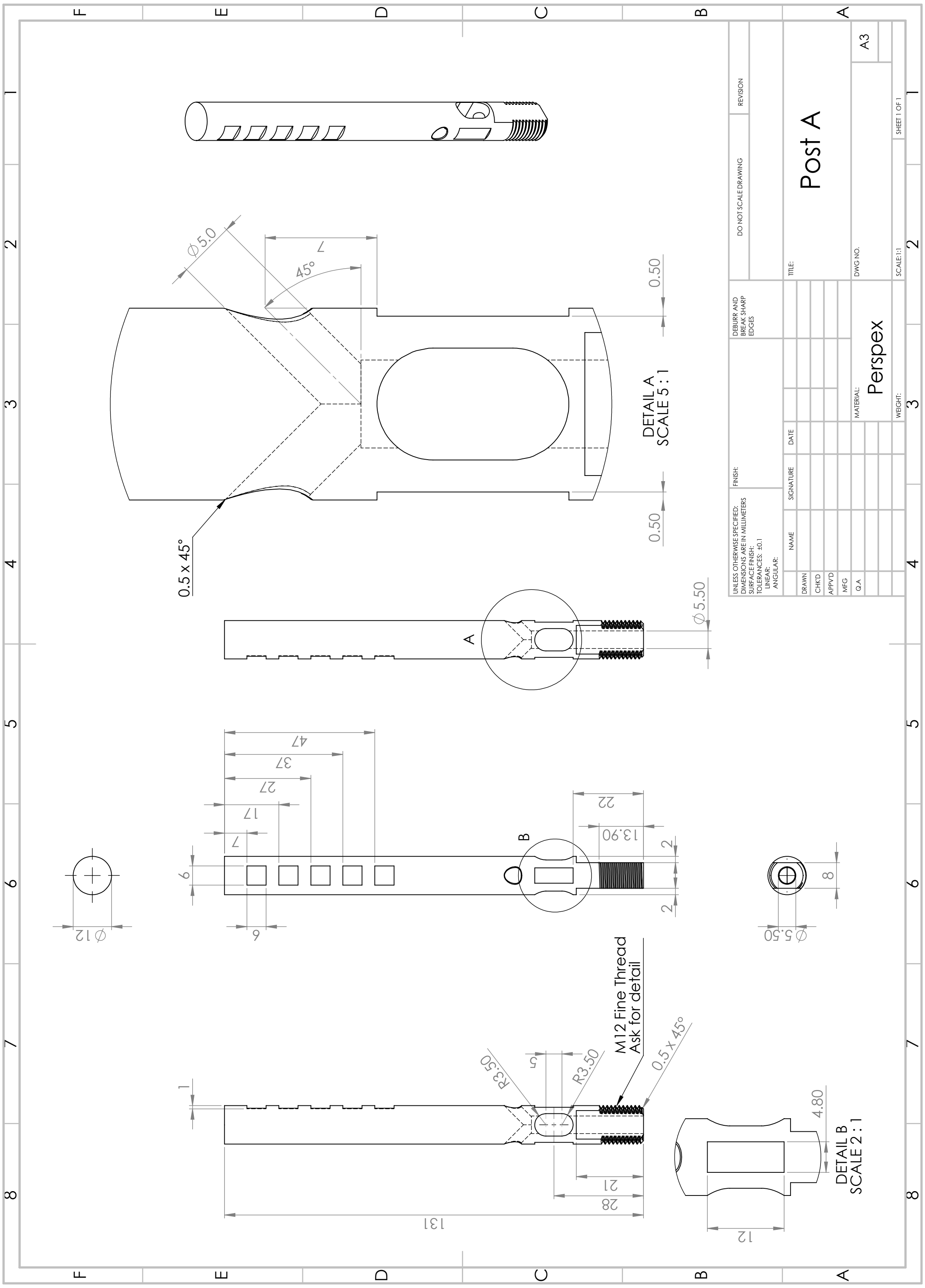

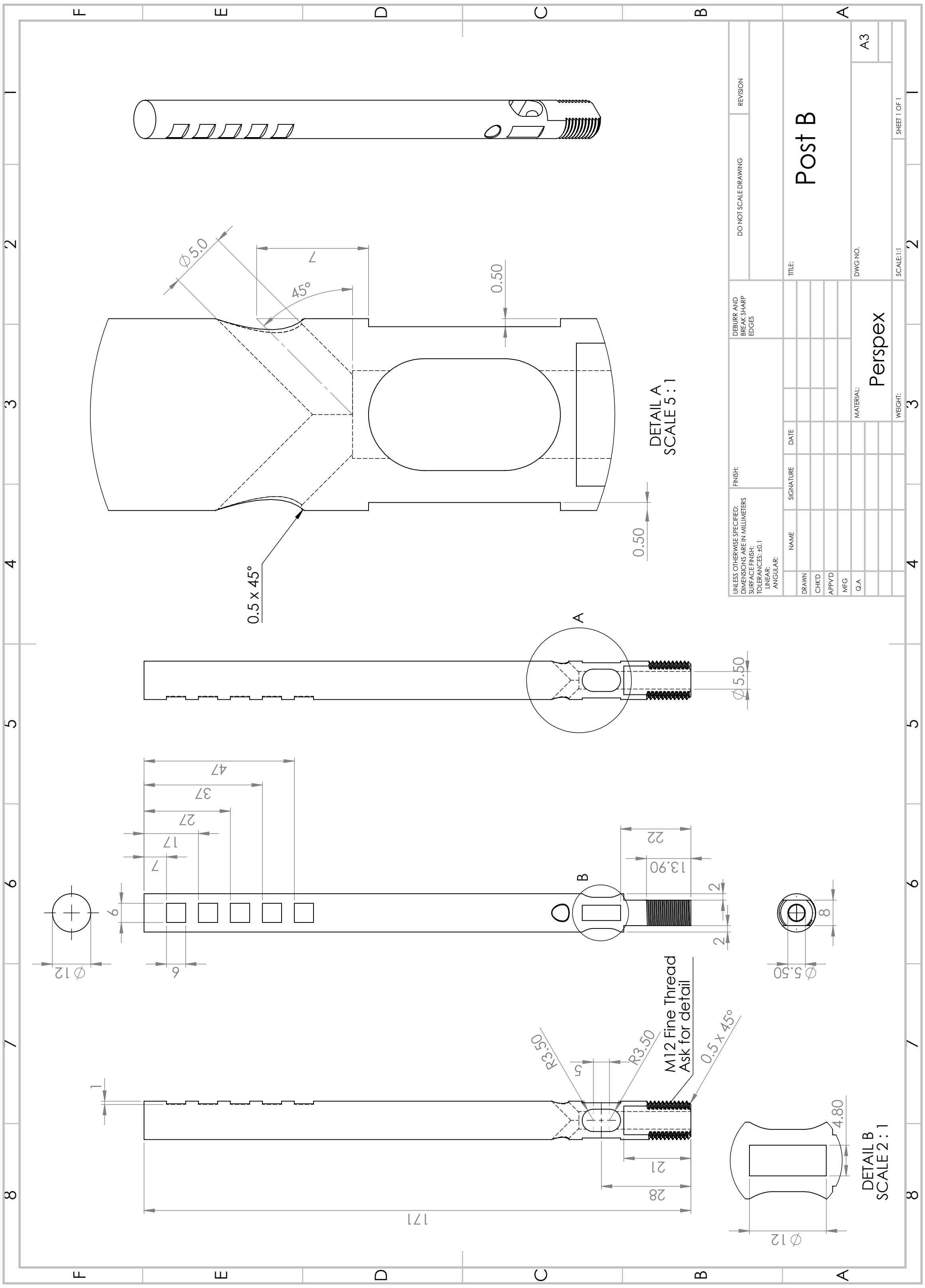
Post B
Perspex
DETAIL A
SCALE 5 : 1
DETAIL B
SCALE 2 : 1
M12 Fine Thread
Ask for detail
0.5 x 45°
UNLESS OTHERWISE SPECIFIED:
DIMENSIONS ARE IN MILLIMETERS
SURFACE FINISH:
TOLERANCES: ±0.1
LINEAR:
ANGULAR:
FINISH:
DEBURR AND BREAK SHARP EDGES
DO NOT SCALE DRAWING
REVISION
NAME
SIGNATURE
DATE
DRAWN
CHK'D
APPV'D
MFG
Q.A
TITLE:
MATERIAL:
DWG NO.
A3
WEIGHT:
SCALE:1:1
SHEET 1 OF 1

B Concepts

A number of functions and possible design options are listed in Table 3.

Table 3: A summary of the possible design features for different functions

Function	**Designs**			
Turbine post cross-section	*Circular*	*Square*	*Triangular*	*Rectangular*
Strain gauge position	*Close to the top*	*Close to the bottom*	*Anywhere else*	
Direction strain gauge leads	*Up*	*Down*		
Routing the strain gauge leads	*External*	*Internal*		
Possibility of 4 different levels of vertical staggering	*9 different sized posts*	*1 post with 9 flat faces*	*2 posts with 5 flat faces with one overlapping flat face*	
Alignment with flow	*Some adhesive material/product (Glue,tape)*	*1 flat face to align with holes in floorboard*	*2 flat faces to align with holes in floorboard*	
Constrain in vertical direction	*Some adhesive material/product (Glue,tape)*	*Nut*	*Clamp*	

2 Tutorial

2.1 Finding the velocity using the continuity equation

An incompressible steady-flow pattern is given by $u = 2x^3z + \ln(y) + z^2/2$ and $v = 2x - y^2/2$. What is the most general form of the third component $w(x, y, z)$, which satisfies the continuity equation?

Soln.

Substituting into the incompressible continuity equation ($\nabla \cdot \overrightarrow{V} = 0$) gives

$$\frac{\partial u}{\partial x} + \frac{\partial v}{\partial y} + \frac{\partial w}{\partial z} = 0 = 6x^2z - y + \frac{\partial w}{\partial z}$$

$$\therefore \quad \frac{\partial w}{\partial z} = y - 6x^2z$$

Upon integration

$$w = yz - 3x^2z^2 + C(x, y)$$

2.2 Checking incompressibility

A velocity field is given by $\overrightarrow{V} = z(3y^2 - 3x^2)\,\hat{\mathrm{i}} + Cxyz\,\hat{\mathrm{j}} + (3xy^2 - x^3)\,\hat{\mathrm{k}}$. Determine the value of the constant C if the flow is to be (a) Incompressible (b) Irrotational

Soln.

(a) Incompressible: we need $\nabla \cdot \overrightarrow{V} = 0 = \dfrac{\partial u}{\partial x} + \dfrac{\partial v}{\partial y} + \dfrac{\partial w}{\partial z}$

$$\therefore -6xz + Cxz = 0 \qquad \rightarrow \qquad C = 6$$

(b) Irrotational: we need $\nabla \times \overrightarrow{V} = 0$

$$\therefore \begin{bmatrix} \hat{\mathrm{i}} & \hat{\mathrm{j}} & \hat{\mathrm{k}} \\ \dfrac{\partial}{\partial x} & \dfrac{\partial}{\partial y} & \dfrac{\partial}{\partial z} \\ u & v & w \end{bmatrix} = 0 = \left(\frac{\partial w}{\partial y} - \frac{\partial v}{\partial z}\right)\hat{\mathrm{i}} + \left(\frac{\partial u}{\partial z} - \frac{\partial w}{\partial x}\right)\hat{\mathrm{j}} + \left(\frac{\partial v}{\partial x} - \frac{\partial u}{\partial y}\right)\hat{\mathrm{k}}$$

The $\hat{\mathrm{i}}$, $\hat{\mathrm{j}}$ and $\hat{\mathrm{k}}$ components should all be checked. The components are:

$$\left(\frac{\partial w}{\partial y} - \frac{\partial v}{\partial z}\right)\hat{\mathrm{i}} = (6xy - Cxy)\,\hat{\mathrm{i}} = 0$$
$$\left(\frac{\partial u}{\partial z} - \frac{\partial w}{\partial x}\right)\hat{\mathrm{j}} = \left((3y^2 - 3x^2) - (3y^2 - 3x^2)\right)\hat{\mathrm{j}} = 0$$
$$\left(\frac{\partial v}{\partial x} - \frac{\partial u}{\partial y}\right)\hat{\mathrm{k}} = (Cyz - 6yz)\,\hat{\mathrm{k}} = 0$$

We need to utilise $\left(\dfrac{\partial w}{\partial y} - \dfrac{\partial v}{\partial z}\right)\hat{\mathrm{i}} = 0$ and $\left(\dfrac{\partial v}{\partial x} - \dfrac{\partial u}{\partial y}\right)\hat{\mathrm{k}} = 0$ to determine C.

$$\therefore (6xy - Cxy)\,\hat{\mathrm{i}} = 0, \quad (Cy - 6y)\,\hat{\mathrm{k}} = 0$$

Thus $C = 6$ again. The flow is incompressible and irrotational.

2.3 Continuity equation in Polar coordinates

Does the velocity field

$$v_r = 4(1 - \frac{1}{r^2})\sin\theta, \qquad v_\theta = 4(1 + \frac{1}{r^2})\cos\theta, \qquad v_z = 0$$

represent a possible incompressible flow? Note that the continuity equation for an incompressible flow in cylindrical coordinates is given as

$$\frac{1}{r}\frac{\partial}{\partial r}(rv_r) + \frac{1}{r}\frac{\partial v_\theta}{\partial \theta} + \frac{\partial v_z}{\partial z} = 0$$

Soln.
The (r, θ, z) coordinates are cylindrical coordinates. The given flow field needs to be verified with the continuity equation in cylindrical coordinates for incompressible fluids:

$$\frac{1}{r}\frac{\partial}{\partial r}(rv_r) + \frac{1}{r}\frac{\partial v_\theta}{\partial \theta} + \frac{\partial v_z}{\partial z} = 0$$

So, we want to know whether the given velocity field satisfies the incompressible form of the continuity equation. If we substitute the velocity components into the equation we have:

$$\frac{4\sin\theta}{r}\frac{\partial}{\partial r}\left(r - \frac{1}{r}\right) + \frac{4}{r}\left(1 + \frac{1}{r^2}\right)\frac{\partial}{\partial \theta}(\cos\theta) + \cancel{\frac{\partial v_z}{\partial z}} \stackrel{?}{=} 0$$

Differentiate and find

$$\frac{4\sin\theta}{r}\left(1 + \frac{1}{r^2}\right) - \frac{4}{r}\left(1 + \frac{1}{r^2}\right)\sin\theta = 0$$

Continuity is satisfied, so the velocity field is a possible incompressible flow.

2.4 Continuity equation in a piston-cylinder flow

A piston compresses gas in a cylinder by moving at constant speed V_0, as in the figure below. Let the gas density and length at $t = 0$ be ρ_0 and L_0, respectively. Let the gas velocity vary linearly from $u = V_0$ at the piston face to $u = 0$ at $x = L$. If the gas density varies only with time, find an expression for $\rho(t)$.

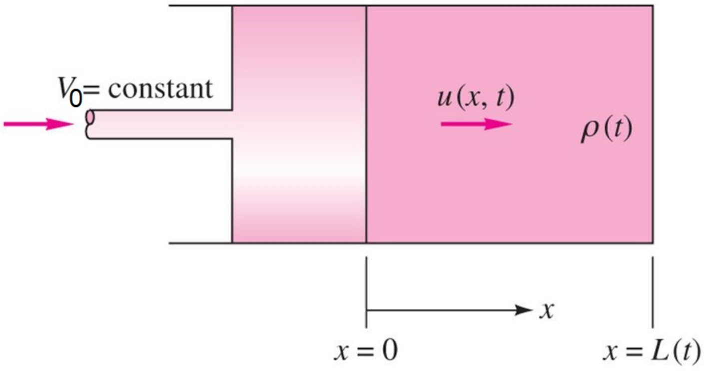

Soln.
The continuity equation

$$\frac{D\rho}{Dt} + \rho(\nabla \cdot \mathbf{v}) = 0$$

$$\frac{\partial \rho}{\partial t} + \cancel{u\frac{\partial \rho}{\partial x}} + \cancel{v\frac{\partial \rho}{\partial y}} + \cancel{w\frac{\partial \rho}{\partial z}} + \rho\left(\frac{\partial u}{\partial x} + \cancel{\frac{\partial u}{\partial y}} + \cancel{\frac{\partial v}{\partial z}}\right) = 0$$

reduces to

$$\frac{\partial \rho}{\partial t} + \rho\frac{\partial u}{\partial x} = 0$$

$$\frac{\partial \rho}{\partial t} = -\rho\frac{\partial u}{\partial x}$$

where $u = V_0(1 - \frac{x}{L})$, $L = L_0 - V_0 t$, and $\rho = \rho(t)$ only. Enter $\frac{\partial u}{\partial x} = -\frac{V_0}{L}$ and separate variables:

$$\int_{\rho_0}^{\rho} \frac{\mathrm{d}\rho}{\rho} = V_0 \int_0^t \frac{\mathrm{d}t}{L} = V_0 \int_0^t \frac{\mathrm{d}t}{L_0 - V_0 t}$$

u-substitution of the above integral using $s = L_0 - V_0 t$ and $\mathrm{d}s = -V_0 \mathrm{d}t$ results in:

$$\int_{\rho_0}^{\rho} \frac{\mathrm{d}\rho}{\rho} = V_0 \int_{L_0}^{L_0 - V_0 t} \frac{1}{-V_0 s}\mathrm{d}s = -\int_{L_0}^{L_0 - V_0 t} \frac{1}{s}\mathrm{d}s$$

The solution is:

$$\ln\left(\frac{\rho}{\rho_0}\right) = -\ln(L_0 - V_0 t) + \ln(L_0) = \ln\left(\frac{L_0}{L_0 - V_0 t}\right)$$

2.5 Bernoulli's equation and conservation of mass in a branched pipe

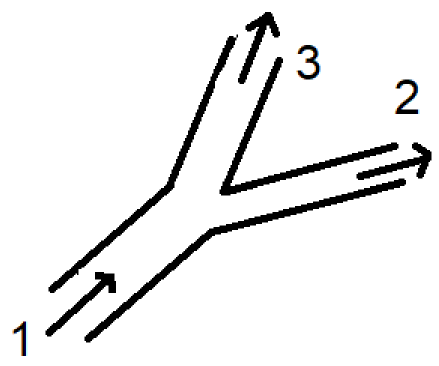

Figure 1: Top view of a branching pipe.

Water flows through a horizontal branching pipe as can be seen in Figure 1. The water enters at the inlet, indicated by 1, and flows out of the pipe at two different outlets, indicated by 2 and 3. The velocity, pressure and area of inlet 1 are $v_1 = 5$ m/s, $p_1 = 400$ kPa and $A_1 = 0.1$ m^2, respectively. The flow is incompressible. Use a density of 1000 kg/m^3 for water.

(a) Using Bernoulli's equation for a streamline, find the velocity at outlet 2 (v_2) if $p_2 = 328$ kPa and $A_2 = 0.02$ m^2.
(b) Use the solution of (a) to find the velocity at outlet 3 (v_3) if the area of outlet 3 is $A_3 = 0.06$ m^2.

Soln.
(a) Bernoulli's equation for a streamline for an incompressible flow reads:

$$\frac{p}{\rho} + \frac{v^2}{2} = \text{constant along a streamline.}$$

Considering a streamline from inlet 1 to outlet 2 gives the relation

$$\frac{p_1}{\rho} + \frac{v_1^2}{2} = \frac{p_2}{\rho} + \frac{v_2^2}{2}.$$

This can be rewritten so that an expression for v_2 is found:

$$v_2^2 = \frac{2(p_1 - p_2)}{\rho} + v_1^2 = \frac{2(400 \cdot 10^3 - 328 \cdot 10^3)}{1 \cdot 10^3} + 5^2 = 169 \text{ m}^2/\text{s}^2.$$

$$\therefore v_2 = \sqrt{169} = 13 \text{ m/s}$$

(b) Use conservation of mass to find the velocity v_3 using:

$$A_1 v_1 = A_2 v_2 + A_3 v_3$$

Rearranging gives

$$V_3 = \frac{(A_1 v_1 - A_2 v_2)}{A_3} = \frac{0.1 \cdot 5 - 0.02 \cdot 13}{0.06} = 4 \text{ m/s}.$$

D Reflection report

D.1 Learning objectives

Before the start of my internship I set some goals for myself. These goals can be categorised into three categories: social skills, academic skills, and the ability to work independently. A valuable learning situation of each category that I experienced during my internship is described below using the STARL method.

Social skill: improving English		
S	Situation	All the tutors discussed the problems for the tutorials of that week during the weekly meetings on Monday. We would sit around a table while the tutor who was in charge of the topic of that week presented the solutions to the problems. If anything is unclear or if one of the tutors reckoned students would struggle to understand some part of the solutions we collaboratively tried to make it more detailed or more clear. The group of tutors consisted of mainly PhD students from different countries and different fields of engineering who were finishing their PhD in the School of Civil Engineering.
T	Task	We were required to point out any error in the solutions or make them more clear in such a way that Civil Engineering students would understand the solutions and also see the value of solving the problems from the tutorials. This was sometimes challenging because the team of tutors are from different engineering departments and our proposed solutions became too technical.
A	Action	I tried to position myself in the shoes of the students and wondered what would be relevant to a student in the field of civil engineering. As one of the youngest in the team of tutors I would be one of the best persons to do so. In order to communicate this to the other tutors I would have to express myself as clearly as possible.
R	Reflect	The first few meetings were somewhat chaotic because most of the tutors, including me, were attending the meeting in silence while two or three tutors were having an active discussion. After a few weeks I was able to take part in the discussion and make some valid points to improve the quality of the problems and the solutions. This was confirmed by the students who were asking questions about the way the solutions were written in the first few weeks while during later tutorials the questions were more about the content instead.
L	Learning	Communication is key to learning. If someone possesses the knowledge but is unable to express himself, this knowledge will not be passed onto the next generation of engineers.

Academic skill: analysing and interpreting data		
S	Situation	I was doing experiments in the wind tunnel and my strain gauge measurements were finalised for a particular set of setups. It was time to start taking streamwise velocity profile measurements using a Cobra probe and in order to validate the data acquired from the Cobra Probe a reference probe was used that was well calibrated. After setting up the velocity profile instruments and running some experiments I noticed that the signal from the reference probe was lower than expected.
T	Task	In order to continue my experiments I had to investigate the cause of the drop in the reference probe.
A	Action	I started by checking the results of the previous experiments and I noticed that the problem arose in a previous experiment. Then I analysed the code that was used to acquire the data during the experiments. It could be that some variables were overwritten during another part of the code that I had overlooked. After making sure this was not the case I starting checking the wiring of the reference probe, and after concluding that the wiring was fine I looked at the probe itself. Apparently one of the soldered wires had come loose inside the probe. I asked one of the technicians to solder the loose wire back on. This solved the problem.
R	Reflect	The actions that were needed in order to solve the reference probe took me longer than expected. This was mainly because checking the code (that was constructed from parts of different codes that used the equipment used in my experiments) was sometimes hard to understand because analysing code that is written by someone else takes time and skill to understand.
L	Learning	Faulty measurement data can be caused by many factors. Always validate that your software data acquisition method works. If a problem still arises after the software check try to look for a problem in the hardware. Another learning moment of mine is that it comes important to validate a code that is written by someone else before using it for my own experience.

Working independently: setting up an experiment and conduct the experiment by myself		
S	Situation	Other than designing the new turbine posts and tutoring in Fluid Mechanics, Kapil left it up to me to choose my research subject that comprises wind turbine experiments in the wind tunnel. This meant that I can come up with my own experiments and also make sure the experiments are finished and documented within the time span on my internship. I chose vertical staggering in wind farms.
T	Task	In order to do my experiments, I have to come up with experiments, do the design of the experimental setup in order to do the experiments and analyse the data acquired during the experiments.
A	Action	I started off by requesting the final design of the posts to be ordered and shipped to the university. I then designed the floorboard including the frame that will be used to position the turbine posts inside the wind tunnel and submitted a working request for the workshop to make the floorboards and to order the frame. Once every component of the setup came in, I tried to assemble everything in the wind tunnel and start the experiments and solve every problem that arose during the experiments. Afterwards I analysed the data.
R	Reflect	Starting with a new research project within an organisation means that you will have to think of everything. This includes the design of the experimental setup, the experiments that you want to conduct and then documenting everything that you have done. At the start of the project I did not have a solid plan and I just tried to solve every problem as it came along. This resulted in me doing my experiments in the last few weeks of the internship and thereby reducing the amount of time I could spend on analysing the data. Many different phenomenon can still be looked at with the data that I got from my experiments.
L	Learning	Planning a set of experiments costs time and effort, and even though you can think about a lot of problems that can arise during the process and can be tackled easily, one small detail that you missed can cause a lot of delay and headaches. Always plan more time for than you originally anticipate on.

D.2 External supervisor feedback

The discussions with Kapil throughout my internship were valuable although they were limited. He gave me great advise on how to set up the experiments and even suggested to do more experiments. He helped me keep on schedule as much as possible and he encouraged me to take initiative in setting up my own experiments.

Krishna helped me analyse the data and suggested more experiments and analysing techniques that have the potential of ending up in a journal paper.

Zach and Theo helped me to make decisions throughout the research project and made sure I thought of every detail before finalising my decision. He had experience with wind farm setups in the wind tunnel and he could offer me some valuable do's and dont's.

D.3 What's next?

Get to know more people from the organisation in order to extend network and thus job potential. My goal is to get to know at least ten people within an organisation in this field of research. Furthermore, in my next research project, I would like to work on my planning skills by setting weekly goals instead of postponing every task and having to make up for the lost time at the end of the project. This will allow me to work normal working hours and increase the potential of my data analysis.